Toward Theranostic Nanoparticles: CB[7]-Functionalized Iron Oxide for Drug Delivery and MRI

Farah Benyettou,[a] Irena Milosevic,[b] Yoann Lalatonne,[b] Fabienne Warmont,[c] Rana Assah,[a] John-Carl Olsen,[d] Mustapha Jouaid,[e] Laurence Motte,[b] Carlos Platas-Iglesias[f] and Ali Trabolsi*,[a]

[a]*New York University Abu Dhabi, Center for Science and Engineering, Abu Dhabi, United Arab Emirates*
[b]*Université Paris 13, Sorbonne Paris Cité, Laboratoire CSPBAT, CNRS, (UMR 7244), F-93017, Bobigny, France*
[c]*Centre de Recherche sur la Matière Divisée (CRMD), Université d'Orléan, CNRS, F-45071, Orléans, France*
[d]*School of Sciences, Indiana University Kokomo, Kokomo, IN 46904, USA*
[e]*Masdar Institute of Science and Technology, Nano labs Division, Abu Dhabi, United Arab Emirates*
[f]*Departamento de Química Fundamental, Universidade da Coruña, Campus da Zapateira, Rúa da Fraga 10, 15008 A Coruña, Spain.*

Supporting Information

*Correspondence Address
Professor Ali Trabolsi *Center for Science and Engineering* New York University Abu Dhabi Abu Dhabi, UAE Tel: (+971)-26284575 Fax: (+971)-26238616 E-Mail: ali.trabolsi@nyu.edu

General Methods

All reagents were purchased from commercial suppliers (Sigma-Aldrich) and used without further purification. Nanopure water (conductivity of 0.06 µS cm^{-1}), obtained from a Millipore Gradiant Elix-3/A10 system was used to prepare the sample solutions. Iron concentration was deduced from ultraviolet-visible absorption spectra recorded with an Agilent Technologies Cary 5000 Series UV-Vis-NIR Spectrophotometer in water at room temperature (298 K). Solutions were examined in 1 cm spectrofluorimetric quartz cells. The experimental error of the wavelength values was estimated to be ±1 nm. Infrared spectra were recorded on an Agilent Technologies Cary 600 Series FTIR Spectrometer using the ATR mode. Size and morphology of the nanoparticles were determined by Transmission Electron Microscopy (TEM, PHILIPS CM20 microscope operating at 200 kV). The powder X-ray diffraction (PXRD) patterns of the samples were collected using a X-ray Panalytical Empyrean diffractometer. The particle size and peak positions were obtained from X-Ray diffraction patterns with HighScore Plus 3.0.5. Hydrodynamic size and ζ-potential measurements were performed on a Malvern Zetasizer NanoSeries. ζ-potential measurements were made on solutions of pH = 2 to 12, using automated titration and sample preparation (MPT-2 Autotitrator, Malvern). Thermogravimetric Analyses were performed on a TA SDT Q600 device. Emission spectra were recorded in water, at room temperature, using an excitation wavelength of 510 nm corresponding to the maximum of absorption of the dye (Nile red, **NR**) using a Perkin Elmer LS55 Fluorescence Spectrometer. Magnetic properties of the nanoparticles were studied using a MIAtek reader® (Magnetic Immunoassays Technology). The transverse nuclear relaxation times, T_2 were measured from axial T_2-weigthed spin-echo (SE) images obtained with a time repetition (TR) of 2,000 ms and increasing time echo (TEs) of 20, 40, 60, and 80 ms with a 1.5 T MRI scanner (Philips intera 1.5T / Philips healthcare) at room temperature for various iron concentrations. Optical and fluorescence images were observed on a LEICA DMI 3000B confocal scanning microscope.

1. Synthesis, characterization and functionalization of γ-Fe$_2$O$_3$ nanoparticles (NPs)

1.1. NP synthesis

NPs (8 ± 1 nm) were synthesized by using a previously reported literature procedure.[1,2] A 40% v/v solution of dimethylamine in water (9.0 mL) was added to an aqueous micellar solution (69.5 mL) of ferrous dodecyl sulfate (1.0 mmol). The mixture was stirred vigorously for 2 h at 28 °C. The resulting precipitate was isolated from the supernatant at pH = 6.7

(which corresponds to the isoelectric point of the uncoated nanoparticles, **NPs**) by magnetic separation and washed with H_2O. Formation of the **NPs** was confirmed by TEM.

1.2. Surface functionalization of NPs with CB[7]
A) Conventional heating

An aqueous solution (1 mL) of **CB[7]** ($n = 3 \times 10^{-5}$ mol) was added to the colloidal suspension (4 mL, $n_{Fe} = 7 \times 10^{-4}$ mol) of **NPs** (**NPs**:**CB[7]** = 1:1000 ratio) and the mixture was stirred for 24 hours at room temperature. **NPs** were precipitated using a magnet and washed with water repeatedly without centrifugation to remove excess of **CB[7]**.

The same functionalization procedure was also conducted at 50 °C in order to determine the effect of temperature. In both cases, iron concentration was deduced from UV-Vis spectroscopy measurements.

B) Microwave heating

An aqueous solution (1 mL) of **CB[7]** ($n = 3 \times 10^{-5}$ mol) was added to the colloidal suspension (4 mL, $n_{Fe} = 7 \times 10^{-4}$ mol) and the mixture was transferred to a 10 mL vessel with a crimp cap and heated by microwave irradiation of 2.45 GHz in a microwave reactor (CEM Discovery, CEM Inc. USA). The power was modulated in order to reach a temperature of 50 °C in one minute and to maintain that temperature for 30 minutes. The maximum power applied was 300 W. Stirring was initiated at 50 °C during the heating cycle. One or two heating cycles were used to prepare **CB[7]NPs**, with two cycles being optimal. The **NPs** were washed with water and precipitated by using a magnet. Iron concentration was deduced from UV/Vis absorption data.

1.3. Encapsulation of Nile Red (NR) by CB[7] on CB[7]NPs

CB[7]NPs ($n_{CB[7]} = 6 \times 10^{-4}$ mol) and **NR** (6×10^{-4} mol) were mixed in water (2 ml) and stirred for two hours at room temperature to form inclusion complexes on the surface of **NPs**. The product was precipitated by using a magnet and washed several times with water; the brown solid was designated **CB[7]NPs⊃NR**. The encapsulation of **NR** was confirmed by FTIR, fluorescence emission spectrometry and ζ-potential measurements.

2. NP Characterization
2.1. Fourier Transform Infrared (FTIR) Spectroscopy

Surface coating of **NPs** was confirmed and characterized an Agilent Technologies Cary 600 Series FTIR Spectrometer. Figure S1 shows the FTIR spectra of A) **CB[7]** B) uncoated γ-**Fe$_2$O$_3$** nanoparticles, **NPs** C) **CB[7]NPs** synthesized at room temperature (24 h) D) **CB[7]NPs** synthesized by conventional heating at 50 °C (24 h) E) **CB[7]NPs** synthesized by microwave heating at 50 °C for 30 minutes F) **CB[7]NPs** synthesized by microwave heating at 50 °C for 2×30 minutes and G) **CB[7]NPs⊃NR**.

The NPs synthesized by two cycles of microwave heating at 50 °C for 30 minutes were used exclusively for all subsequent studies involving adsorption of CB[7] and encapsulation of NR.

Figures S1A and S1B show the FTIR absorption spectra of **CB[7]** molecules and **NPs. CB[7]** is symmetrical, with two identical carbonylated portals that give rise to a single C−O stretching vibration at 1723 cm^{-1}. Additional absorption bands that correspond to C−H, N−H and C−C vibrations in **CB[7]** are also present in the spectrum. Contact with **NPs** desymmetrizes **CB[7]** and gives rise to two distinct C=O absorption peaks at 1734 and 1633 cm^{-1} which are apparent in Figures S1(C-F).

Figure S1G shows a spectrum of **CB[7]NPs** (*obtained from microwave heat at 50 °C for 2 cycles of 30 minutes*) after complexation with **NR**. The similarity of this spectrum to that shown in Figure S1F indicates that **CB[7]** remains on the surface of the **NPs** after host-guest complexation.
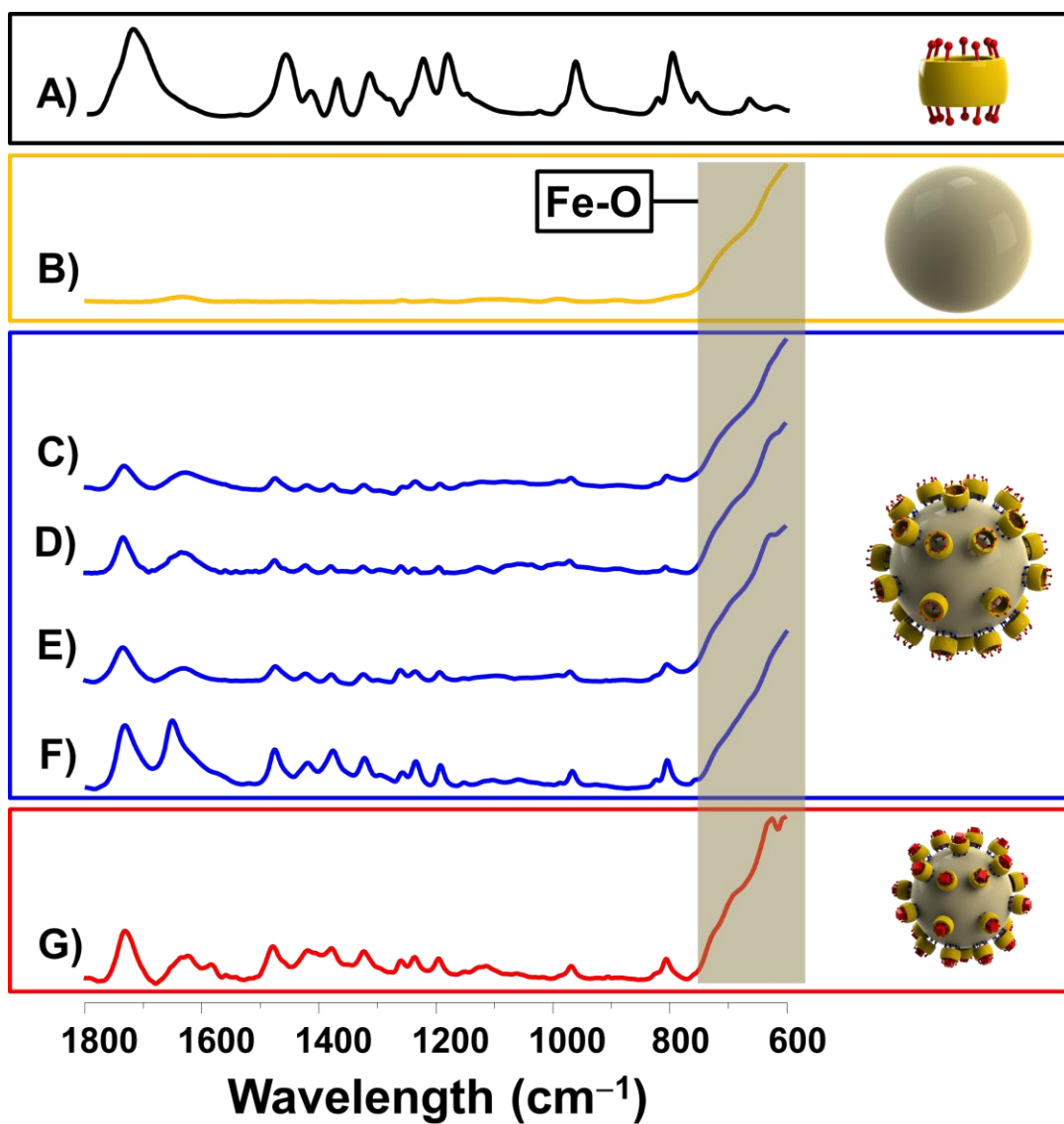
Figure S1 FTIR spectra of A) **CB[7]** B) uncoated γ-Fe_2O_3 nanoparticles, **NPs** C) **CB[7]NPs** synthesized at room temperature for 24 h D) **CB[7]NPs** synthesized by conventional heating at 50 °C for 24 h E) **CB[7]NPs** synthesized by microwave heating at 50 °C for 30 minutes F) **CB[7]NPs** synthesized by microwave heating at 50 °C for 2×30 minutes and G) **CB[7]NPs⊃NR**.

Figure S2 displays the FTIR spectra of **CB[7]NPs** at pH = 3, 7 and 12. These results clearly showed the presence of complexed **CB[7]** on the **NPs** surface all over the pH range.
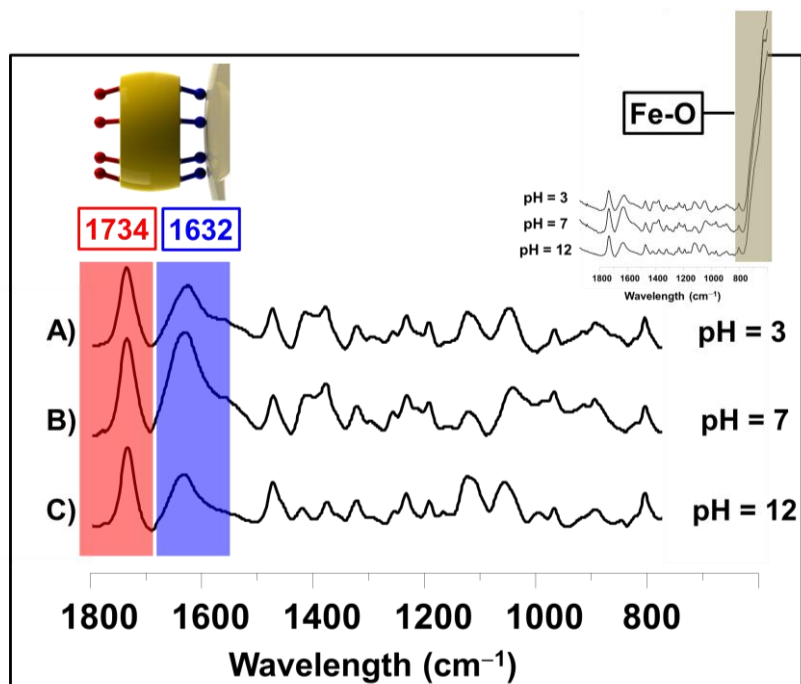
Figure S2 FTIR spectra (800 – 1800 cm^{-1}) of **CB[7]NPs** at A) pH = 3 B) pH = 7 and C) pH = 12. Inset: FTIR spectra (600 – 1800 cm^{-1}) of **CB[7]NPs** at different pH that display the Fe-O bond used as a reference. The three spectra were normalized using the Fe-O bond.

2.2. Transmission Electron Microscopy (TEM) and Powder XRD (PXRD)

Size and morphology of the nanoparticles were determined with a PHILIPS CM20 microscope operating at 200 kV. Samples were prepared on a carbon-coated copper grid. A drop of **NP** solution ([Fe]= 1.0×10^{-5} M) was spotted on the grid and allowed to dry overnight. Figure S3A shows **NPs** before (A, B) and after (D, E) surface functionalization with **CB[7]**. The particle size distribution was determined using a standard methodology.[3] In both cases the nanoparticles are 8 ± 1 nm in diameter and present a spherical shape.
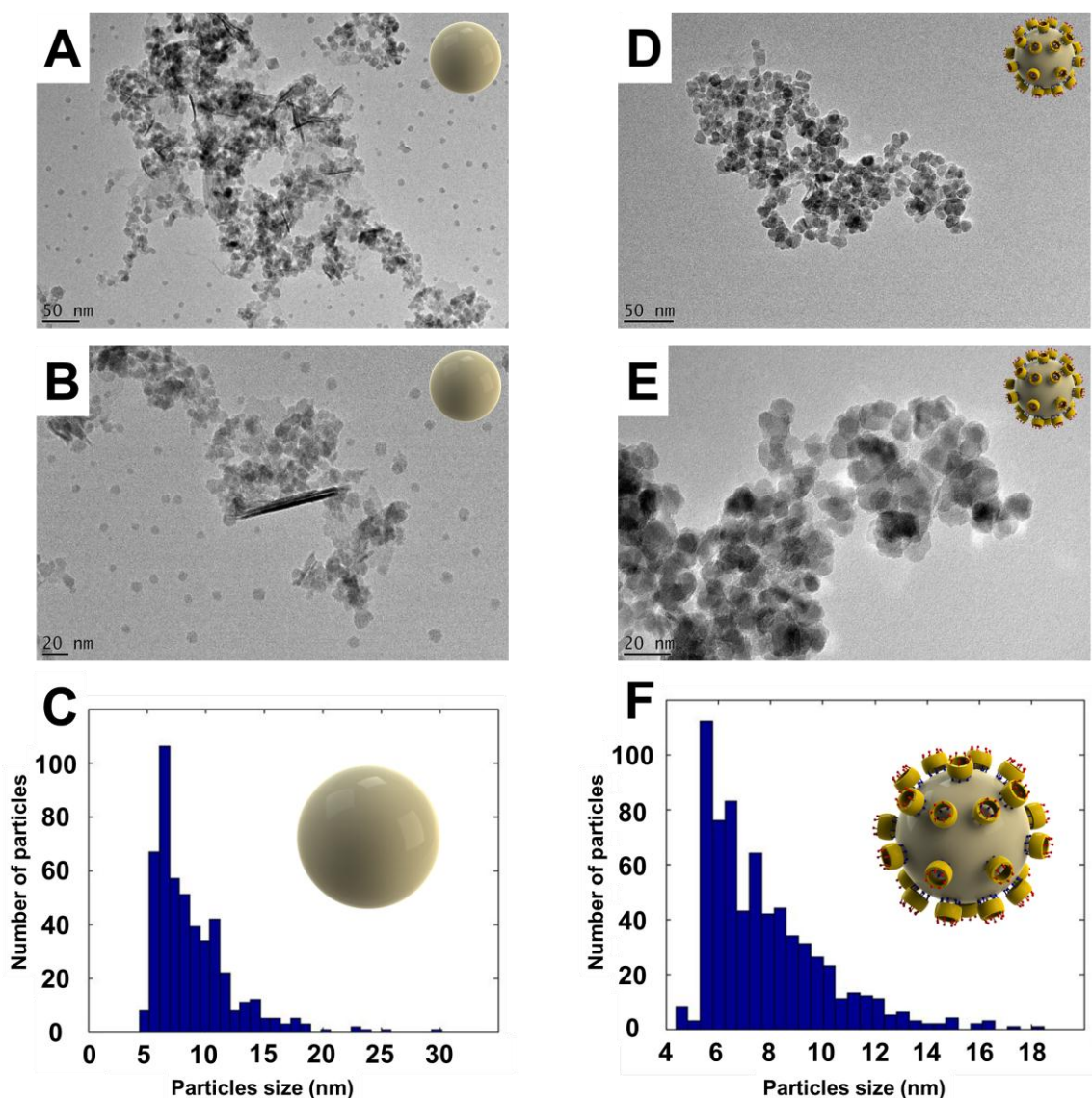
Figure S3. HRTEM images of **NPs** (A, B), and **CB[7]NPs** (D, E). Histograms show the particles size distribution of **NPs** (C) and **CB[7]NPs** (F).

2.3. Dynamic Light Scattering (DLS) Characterization

DLS measurements were carried out on a Zetasizer Nano-ZS (Malvern Instruments) to determine hydrodynamic size and ζ-potential. All samples were analyzed at room temperature in water with diluted ferrofluid ([Fe] = 1×10^{-3} M). Figure S4 illustrates the ζ-potential measurements performed at pH = 2 to 12 using automated titration and sample preparation (MPT-2 Autotitrator, Malvern).
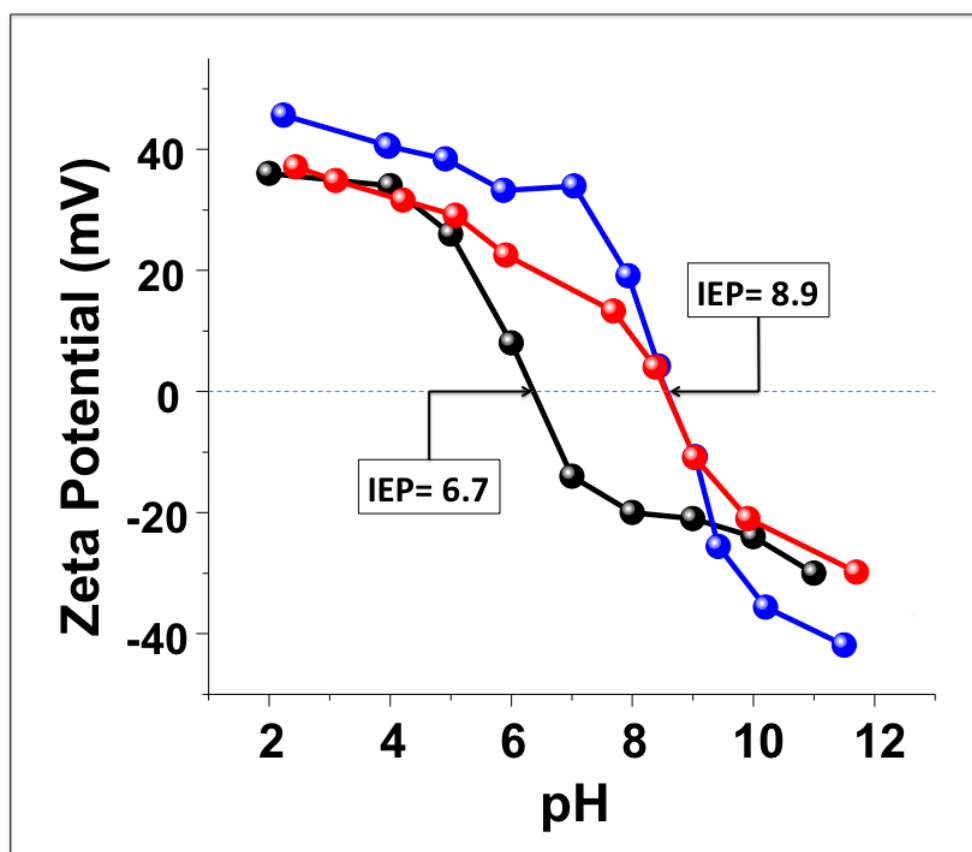
Figure S4. ζ-potential measurements as function of the pH of **NPs** (black curve), **CB[7]NPs** (blue curve) and **CB[7]NPs⊃NR** (red curve).

2.4. Thermogravimetric Analysis (TGA)

The weight percentage (Table S1) of **CB[7]** on the surface of **CB[7]NPs** was determined by TGA. Solid samples (10 mg) under $N_2(g)$ flux were characterized with a SDT Q600 TA Instruments analyzer at a heating rate of 5°C/min over a temperature range of 35−700 °C. Figure S5A shows the weight losses of the **γ-Fe₂O₃ NPs**, and **CB[7]NPs**. The TGA analysis of **CB[7]NPs** shows a composition of 94.84 % iron oxide and 4.33 % of **CB[7]**. With the following equation, these percentages can be used to calculate the number of **CB[7]** macrocycles per **NP**.

	Weight loss (%)	Mass in 1 g (g)	n in 1 g (mol)	Number of entity in 1 g
γ-Fe₂O₃ (NPs)	94.84	$m_{Fe_2O_3} = 0.95$	$n_{Fe} = 12 \times 10^{-3}$	$^{*}N_{nano} = 1.7 \times 10^{18}$
CB[7]	4.33	0.04	4.0×10^{-5}	2.5×10^{19}

Table S1. TGA calculations for **NPs** and **CB[7]NPs** nanoparticles.

$$N_{nano} = \frac{n_{Fe2O3} \times M_{Fe2O3}}{\rho \times \frac{4}{3} \times \pi \times R^3}$$

(*) Where R is the radius of **NP**, as obtained from TEM analysis, ρ is their density, M_{NPs} is the molar mass of γ-Fe_2O_3, and n_{NPs} is the number of moles of **NPs** as deduced from TGA analysis.[4] An average number of 27 **CB[7]** molecules per nanoparticle can be calculated. This result is in reasonable agreement with theory which predicts that the surface of an NP that has a diameter of 8 nm would be able to. If we consider the surface of a nanoparticle with a diameter of 8 nm (surface area = 200.96 nm^2) would be able to accommodate a maximum of 25 molecules of **CB[7]**. We therefore conclude that the density of the nanoparticle coverage is nearly 100 %.

Figure S5 presents the weight losses of **CB[7]NPs** before (red curve) and after (black curve) encapsulation of the **NR** dye. An additional weight loss that corresponds to **NR** can be observed and is consistent with an equimolar complexation of **NR** with **CB[7]**. These data clearly testify to the successful encapsulation of **NR** into the cavities of the **CB[7]** macrocycles.
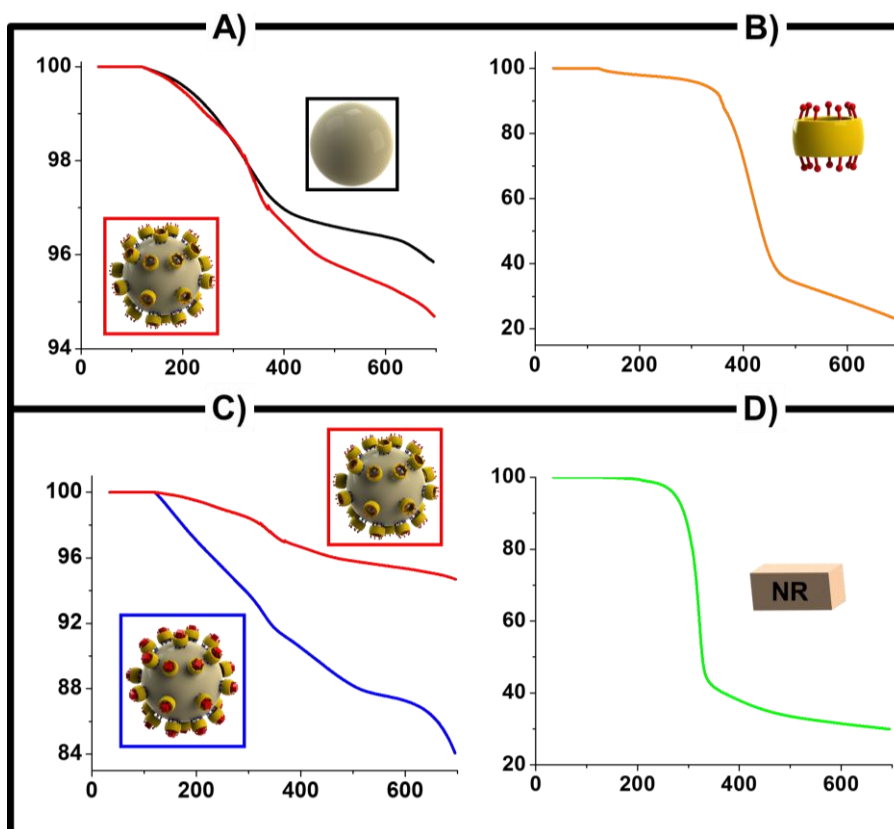
Figure S5 TGA curves of A) **NPs** (black curve) and **CB[7]NPs** (red curve), B) **CB[7]** (orange curve). C) **CB[7]NPs** (red curve) and **CB[7]NPs**⊃**NR** (blue curve) and D) **NR** (green curve).

2.5. Fluorescence emission spectroscopy

Fluorescence from $\textbf{CB[7]NPs} \supset \textbf{NR}$ nanoparticles was measured by a Perkin Elmer LS55 Fluorescence Spectrometer using 510 nm as the excitation wavelength (maximum of absorption of **NR**). It is well known that **NR** does not fluoresce in water but emits red fluorescence in a hydrophobic environment.[5] Fluorescence measurements showed characteristic emission (λ_{max} = 650 nm) of **NR** in water at pH = 7 upon encapsulation with **CB[7]** (**CB[7]** $\supset$ **NR**, Figure S6). By adjusting the pH to 12, the added sodium ions ($[Na^+]$ = 10^{-2} M) compete with **NR** for the carbonyl portal of **CB[7]** and consequently diminish the **NR** fluorescence signal. This result is confirmed by the addition of NaCl, which causes a similar decrease of the fluorescence intensity over time.
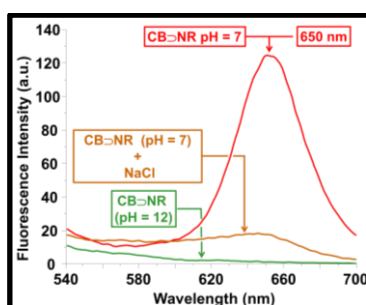
Figure S6A Fluorescence emission spectra of **CB[7]** $\supset$ **NR** at pH = 7 (red curve), **CB[7]** $\supset$ **NR** at pH= 12 (green curve), **CB[7]** $\supset$ **NR** at pH = 7 in presence of NaCl (orange curve), (Solvent: H_2O, room temperature, λ_{ex} = 510 nm).

In serum: An aqueous solution (100 μL) of **CB[7]NPs** $\supset$ **NR** ($[Fe]$ = $1,6 \times 10^{-1}$ M, n_{Fe}= $1,6 \times 10^{-5}$ mol, $n_{CB[7]}$ = 2×10^{-8} mol) was added to 3 mL of Fetal Bovine Serum (FBS). The mixture was stirred for twenty-four hours at room temperature. The product was then precipitated by centrifugation and washed with water.

For fluorescence measurements recorded in water, the solution was diluted 3 times and compared to those that were measured at the same concentration but had not been incubated in serum. Fluorescence measurements show no significant decrease of emission intensity of NR, an indication that NR remains in the cavity of CB[7]. The hydrodynamic diameter of **CB[7]NPs** $\supset$ **NR** in pure serum was measured and found to be d = 25.17 nm (IDPs = 0.33). d = 24.21 nm after washing with water.
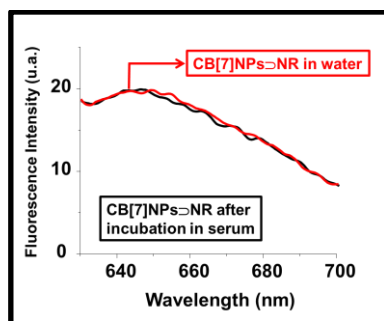
Figure S6B: comparison of the emission spectra of CB[7]NPs-NR before (red) and after (black) incubation in FBS for 24 hours at room temperature. Both spectra were recorded in water at room temperature using λ_{ex} = 510 nm.

	Hydrodynamic Size d (nm)	Zeta-potential (ζ)
CB[7]NPs⊃NR in FBS	25.17	−6.4
CB[7]NPs⊃NR in H_2O (after removing FBS)	24.17	−3.6

Table S2. Hydrodynamic size and zeta potential values of **CB[7]NPs⊃NR** in pure FBS after 24 hours, and in water after the removal of FBS.

2.6. Magnetic properties study (MIAtek®)

Magnetic properties of the nanoparticles, **NPs** and **CB[7]NPs⊃NR**, were studied using a MIAtek® reader (Magnetic Immunoassays Technology), which measures a signal proportional to the third derivative of magnetization at zero magnetic field. The detection method was based on the nonlinear magnetization of superparamagnetic iron oxide nanoparticles. An alternating magnetic field was applied to the sample at two different frequencies $f_1 = 100$ kHz and $f_2 = 100$ Hz having amplitudes of 10 and 200 Oe, respectively. The response of the sample was measured at combinatorial frequencies, e.g., $f = f_1 \pm 2{\times}f_2$.[6] Compared to **NPs**, **CB[7]NPs** and **CB[7]NPs⊃NR** are less aggregated as a consequence of having more positive charge on their surface. This difference explains the increase of the Miatek® Signal assembled in Table S3.

	NPs	CB[7]NPs	CB[7]NPs⊃NR
Miatek Signal (a.u./mg)	189,253	444,846	551,225

Table S3. MIAtek® signal of **NPs**, **CB[7]NPs**, and **CB[7]NPs⊃NR**.

2.7. MRI Contrast Agent Evaluation

The ^{1}H NMR relaxometric characterization was performed by measuring the transverse nuclear relaxation times T_2, on a 1.5 T MRI scanner. The measurements were performed at room temperature for various iron concentrations between 0.07 and 0.25 mM. T_2 maps were calculated assuming a monoexponential signal decay and accordingly from four SE images with a fixed TR of 2,000 ms and TE values of 20, 40, 60, and 80 ms. The signal intensity for each pixel as a function of time was expressed as follows: SIpixel xy (t)= So (pixel xy) exp ($-t/T_2$pixel xy). T_2 relaxation times were then deduced by ROI measurements using Image J software. The efficiency of MRI contrast agent was determined by measuring the relaxivities R_2 defined as $R_2 = [(1/T_2)_{meas} = (1/T_2)_{dia}]/C$, where $(1/T_2)_{meas}$ is the value measured with the sample at concentration C of iron, and $(1/T_2)_{dia}$ refers to the nuclear relaxation rate of the diamagnetic host solution (water in our case). The signal intensity of T_2 weighted images

changed substantially with an increasing amount of nanoparticles (Figure S7A), indicating that the nanoparticles generated MR contrast on transverse (T_2) proton relaxation times weighted sequences. Figure S6B shows the relaxation rate $1/T_2$ as a function of the iron concentration. As expected, the relaxation rates varied linearly with the iron concentration. The transverse R_2 relaxivities (corresponding to the slopes of the lines) for the **CB[7]NPs** and **CB[7]NPs⊃NR** nanoparticles are reported in Figure S7B.
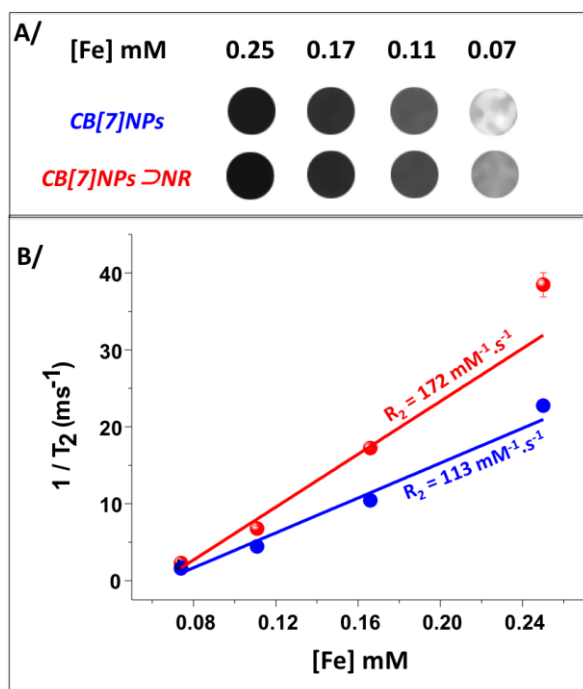
Figure S7. T_2 weighted MR images of aqueous solutions of A) **CB[7]NPs** and **CB[7]NPs⊃NR** at various iron concentrations ([Fe]) and B) T_2 relaxation rates ($1/T_2$) plotted against the [Fe] for the various aqueous solutions of **CB[7]NPs** (blue) and **CB[7]NPs⊃NR** (red).

2.8. Cell lines and culture

HCT116 human colon carcinoma cells were obtained from the American Tissue-Type Culture Collections (ATCC). The cell line was grown in McCoy's 5A medium supplemented with 10 % fetal bovine serum (FBS), at 37 °C in a 5 % CO_2 humidified incubator.

2.9. *In vitro* studies cellular uptake:
The intracellular uptake of **CB[7]NPs** (Figure S8) and **CB[7]NPs⊃NR** was examined using fluorescence microscopy and Prussian blue staining (**CB[7]** and **NR** concentrations = 5 μM) using HCT116 cells. HCT116 cells were seeded in Petri dishes (Ø 30 mm, density 2×10^5 cells per Petri dish), grown for 24 h and treated for 6 h with **CB[7]NPs** and **CB[7]NPs⊃NR** nanoparticles. The cells were then washed three times with PBS, fixed with paraformaldehyde (10 min) and dried at room temperature. The attached cell monolayer was incubated with 5% potassium ferrocyanide (5 min), washed with PBS and

then incubated again with a solution containing 5% potassium ferrocyanide and 10% hydrochloric acid for 10 min and washed with PBS three times. Staining (bright blue pigment) results from the reaction between the Fe^{3+} ions present in the nanoparticles and the ferrocyanide ions. The iron particles in the cells were observed as blue dots using an optical microscope with phase contrast. The experiment was performed in triplicate.
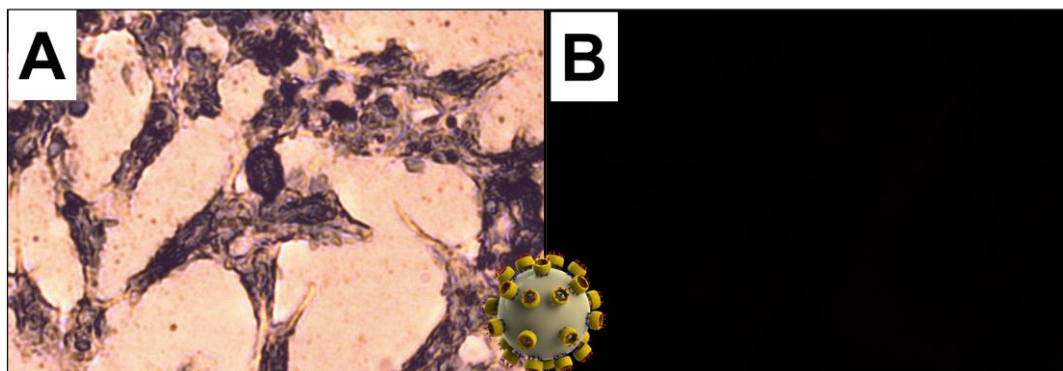
Figure S8. Optical (A) and fluorescence (B) microscopy images of HCT116 cells treated with **CB[7]NPs**.

2.10 *In vitro* cytotoxicity assay. Cell viability was evaluated using the Promegas CellTiter-Blue® Cell Viability assay. It uses the indicator dye resazurin to measure the metabolic capacity of cells—an indicator of cell viability. Viable cells retain the ability to reduce resazurin into resorufin, which is highly fluorescent. Nonviable cells rapidly lose metabolic capacity, do not reduce the indicator dye, and thus do not generate a fluorescent signal. HCT116 cells were seeded at a density of 5.10^4 cells per well in 96-well flat-bottom plates and incubated in 10 % FBS-medium for 24 h. Then, medium was removed and replaced by 10 % FBS-medium containing free **CB[7]** and **CB[7]NPs** increasing **CB[7]** concentrations from 100 µM to 1 µM. After 24 h incubation, cells were washed with phosphate buffered saline (PBS, Amresco Biotechnolgy grade) and incubated with 20 µL of CellTiter-Blue® Reagent for additional 6 h at 37 °C. The fluorescence corresponding to the resorufin (which reflects the relative viable cell number) was measured at 590 nm using a Synergy H1 Hybrid Reader Biotek. The measurement was performed on untreated cells as a blank control.
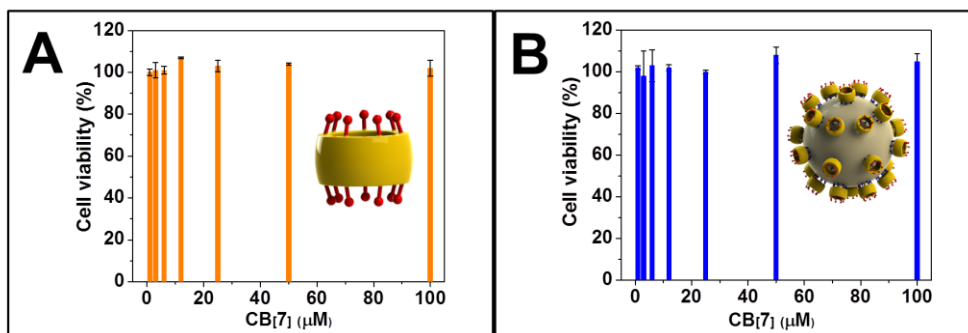
Figure S9. Neither **CB[7]** nor **CB[7]NPs** displayed cytotoxic effects after 24 h of incubation at concentrations as high as 100 μM.

2.11. Computational Details.

All calculations presented in this work were performed employing the Gaussian 09 package (Revision B.01).[7] Full geometry optimizations of the **1**, $(\mathbf{1})_2 \cdots OH_2$, $\mathbf{1} \cdots (H_2O)Fe(OH)_3$ and **1**-$Fe(OH)_3$ systems were performed employing DFT within the hybrid meta-GGA approximation with the TPSSh exchange-correlation functional[8] and they are summarized in Figure S10. In these calculations we used the standard Ahlrichs' valence triple-ξ basis set including polarization functions (TZVP).[9] No symmetry constraints have been imposed during the optimizations. The stationary points found on the potential energy surfaces as a result of geometry optimizations were tested to represent energy minima rather than saddle points via frequency analysis. The default values for the integration grid (75 radial shells and 302 angular points) and the SCF energy convergence criteria (10^{-8}) were used in all calculations. The two systems containing Fe(III) were modeled in their high-spin configurations ($S = 5/2$) using an unrestricted model.[10] Thus, spin contamination was assessed by comparison of the expected difference between $S(S+1)$ for the assigned spin state ($S = 5/2$) and the actual value of $\langle S^2 \rangle$.[10] The results indicate that spin contamination is negligible ($\langle S^2 \rangle - S(S+1) < 0.0071$) in both cases.

The IR absorption profiles were calculated by the formula:

$$A(E) = \sum_i \frac{2.174 \times 10^9 I_i}{\Delta_{1/2}} exp(-2773(E - E_i)^2 / \Delta_{1/2}^2)$$

where the sum runs over all calculated IR frequencies with energies E_i (in cm^{-1}) and IR intensities I_i, obtained using analytical second derivatives, and $\Delta_{1/2}$ represents the half-bandwidths. Thus, the total integrated intensity under the absorption profile equals the sum of

the IR intensities, $\sum_i I_i$.[11] Simulated spectra were obtained using $\Delta_{1/2}$ values of 30 cm^{-1} for all bands, except those corresponding to the carbonyl stretching vibrations, for which $\Delta_{1/2}$ was set to 50 cm^{-1}. Throughout this work a scaling factor of 0.97 was applied to improve the agreement between theoretical and calculated spectra.

1

1-Fe(OH)$_3$

(**1**)$_2$···OH$_2$

1···(H$_2$O)Fe(OH)$_3$
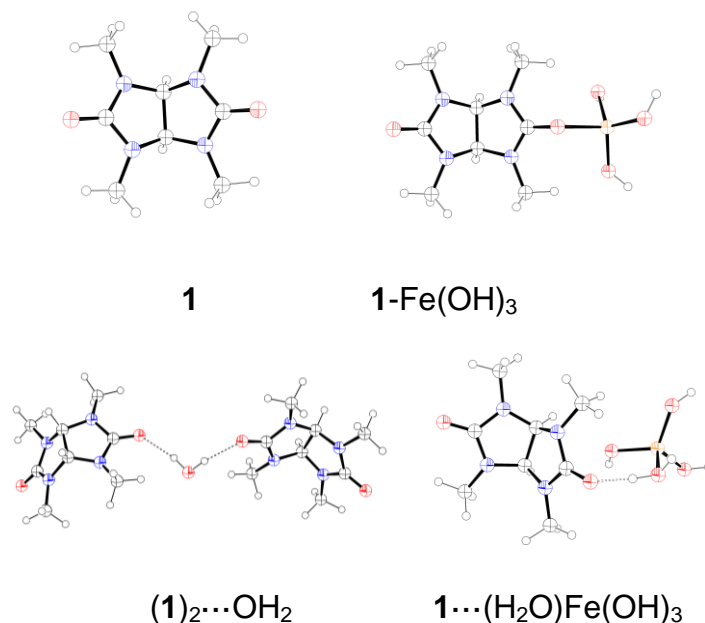
Figure S10. Geometries of the model systems obtained by using DFT calculations (TPSSh/TZVP).

Figure S11 displays the calculated FTIR spectrum of (**1**) used as a model for **CB[7]**.
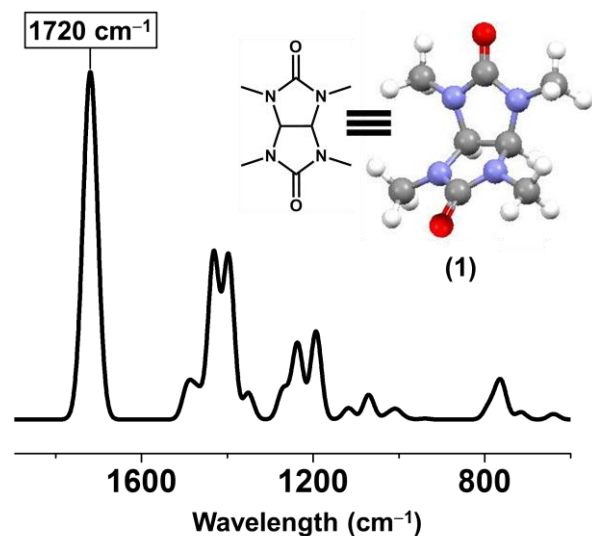
Figure S11. Calculated FTIR spectra of (**1**).

1: TPSSh/TZVP, 0 imaginary frequencies

```
-----------------------------------------------------------------
 Center      Atomic                           Coordinates (Angstroms)
 Number      Number                       X           Y           Z
```

```
          --------------------------------------------------------------------
          1            8                    2.047047   -4.042576   -3.105306
          2            8                    1.731339   -3.830062    3.129346
          3            7                    3.311092   -4.225096   -1.160946
          4            7                    1.245006   -5.095383   -1.189356
          5            7                    3.142877   -4.062169    1.292631
          6            7                    1.164907   -5.115426    1.275337
          7            6                    4.521740   -3.640075   -1.692155
          8            1                    4.416499   -3.499260   -2.747615
          9            1                    5.347442   -4.292911   -1.500005
         10            6                    2.177236   -4.393225   -1.951558
         11            6                    0.045910   -5.629485   -1.798238
         12            1                    0.030090   -5.375462   -2.837527
         13            1                    0.035265   -6.694052   -1.691071
         14            6                    3.213613   -4.898249    0.112545
         15            1                    4.035632   -5.624378    0.215846
         16            6                    1.798007   -5.573058    0.061701
         17            1                    1.842400   -6.673740    0.055078
         18            6                    4.286186   -3.412359    1.891593
         19            1                    5.124949   -4.076416    1.871470
         20            1                    4.059558   -3.154623    2.905058
         21            6                    1.974649   -4.265903    2.023861
         22            6                   -0.080203   -5.625556    1.799830
         23            1                   -0.101330   -6.690311    1.696146
         24            1                   -0.164289   -5.366220    2.834516
         25            1                   -0.897505   -5.198098    1.257431
         26            1                    4.520626   -2.524880    1.341758
         27            1                    4.697300   -2.695070   -1.222002
         28            1                   -0.814305   -5.213887   -1.316357
          --------------------------------------------------------------------
E(RTPSSh) = -683.034335803 Hartree
Zero-point correction = 0.232730
Thermal correction to Energy = 0.247251
Thermal correction to Enthalpy = 0.248195
Thermal correction to Gibbs Free Energy = 0.191329
Sum of electronic and zero-point Energies = -682.808515
Sum of electronic and thermal Energies = -682.793995
Sum of electronic and thermal Enthalpies = -682.793050
Sum of electronic and thermal Free Energies = -682.849917
```

1-Fe(OH)₃: TPSSh/TZVP, 0 imaginary frequencies

Center Number	Atomic Number	Atomic Type	X	Y	Z
			Coordinates (Angstroms)		
1	8		-3.808151	0.211798	1.805822
2	8		1.525283	-0.282789	-1.060089
3	7		-2.688410	1.175091	0.020797
4	7		-2.591503	-1.048963	0.276408
5	7		-0.411971	0.986501	-0.907306
6	7		-0.570909	-1.230251	-1.115475
7	6		-2.966209	2.555019	0.367758
8	1		-3.817396	2.552997	1.047819
9	1		-3.221223	3.119413	-0.533102
10	6		-3.100186	0.125737	0.820331
11	6		-3.205280	-2.323091	0.611978
12	1		-3.830080	-2.155964	1.488754
13	1		-3.830087	-2.689349	-0.212330
14	6		-1.849641	0.748721	-1.064069
15	1		-2.188424	1.180178	-2.012656
16	6		-1.956682	-0.807243	-1.001783

```
     17              1                 -2.544654    -1.246154    -1.816178
     18              6                  0.212017     2.278550    -1.178605
     19              1                  0.172369     2.517494    -2.247932
     20              1                  1.248712     2.242794    -0.838101
     21              6                  0.282537    -0.178163    -1.009473
     22              6                 -0.122151    -2.608014    -0.997584
     23              1                 -0.753960    -3.246384    -1.618444
     24              1                  0.904778    -2.655776    -1.355896
     25              1                 -0.149433    -2.950544     0.039946
     26              1                 -0.307446     3.052932    -0.616371
     27              1                 -2.119558     3.034238     0.868733
     28              1                 -2.450688    -3.073810     0.851245
     29             26                  3.109254    -0.437666    -2.375660
     30              8                  3.560006     1.332532    -2.692476
     31              8                  4.301573    -1.344050    -1.294165
     32              8                  2.507205    -1.359282    -3.841513
     33              1                  2.787882    -2.270345    -3.986849
     34              1                  5.109251    -0.899818    -1.009785
     35              1                  3.490139     1.663369    -3.596155
     ------------------------------------------------------------------
```

E(UTPSSh) = -2174.42932006 Hartree
Zero-point correction = 0.272029
Thermal correction to Energy = 0.295284
Thermal correction to Enthalpy = 0.296228
Thermal correction to Gibbs Free Energy = 0.216075
Sum of electronic and zero-point Energies = -2174.162308
Sum of electronic and thermal Energies = -2174.139052
Sum of electronic and thermal Enthalpies = -2174.138108
Sum of electronic and thermal Free Energies = -2174.218262

1···H_2O-Fe(OH)$_3$: TPSSh/TZVP, 0 imaginary frequencies

```
------------------------------------------------------------------
Center      Atomic                      Coordinates (Angstroms)
Number      Number                  X            Y            Z
------------------------------------------------------------------
      1              8                  3.256666    -2.358005    -1.199067
      2              8                 -0.264481     2.242425     0.337589
      3              7                  3.573193    -0.176573    -0.471638
      4              7                  2.013901    -1.425941     0.530143
      5              7                  1.911091     1.620588    -0.148574
      6              7                  0.815406     0.515331     1.451335
      7              6                  4.502122     0.214057    -1.512376
      8              1                  4.979478    -0.693166    -1.880855
      9              1                  5.262077     0.880739    -1.096935
     10              6                  2.969357    -1.426187    -0.469103
     11              6                  1.420135    -2.661715     1.008426
     12              1                  1.760241    -3.457327     0.345796
     13              1                  1.749421    -2.881265     2.031542
     14              6                  2.922402     0.733550     0.430061
     15              1                  3.661268     1.321596     0.987247
     16              6                  2.060774    -0.208487     1.317874
     17              1                  2.484929    -0.401488     2.310297
     18              6                  2.248362     2.835296    -0.870130
     19              1                  2.997307     3.420634    -0.322522
     20              1                  1.335891     3.422263    -0.966677
     21              6                  0.716398     1.512248     0.526969
     22              6                 -0.307496     0.049330     2.254467
     23              1                  0.087853    -0.399087     3.168108
     24              1                 -0.917962     0.910970     2.524799
     25              1                 -0.915880    -0.673126     1.705998
     26              1                  2.632264     2.605698    -1.865004
```

27	1	4.006309	0.711407	-2.352721
28	1	0.330602	-2.606477	0.978146
29	26	0.639627	6.013380	1.737017
30	8	0.646513	6.488211	3.501542
31	8	2.217377	5.178788	1.230941
32	8	-0.135617	7.148253	0.496811
33	1	-0.161132	8.107434	0.573599
34	1	2.807037	4.922580	1.951903
35	1	0.006377	7.088466	3.899551
36	8	-0.854100	4.607439	1.321549
37	1	-1.423057	5.054159	0.678480
38	1	-0.610579	3.714030	0.941028

E(UTPSSh) = -2250.89837472 Hartree
Zero-point correction = 0.296555
Thermal correction to Energy = 0.322557
Thermal correction to Enthalpy = 0.323501
Thermal correction to Gibbs Free Energy = 0.236098
Sum of electronic and zero-point Energies = -2250.607679
Sum of electronic and thermal Energies = -2250.581677
Sum of electronic and thermal Enthalpies = -2250.580733
Sum of electronic and thermal Free Energies = -2250.668136

$(\mathbf{1})_2 \cdots OH_2$: TPSSh/TZVP, 0 imaginary frequencies

Center Number	Atomic Number	Coordinates (Angstroms) X	Y	Z
1	8	-8.212428	0.168666	0.158505
2	8	-2.246074	-0.270446	1.172102
3	7	-6.256476	1.207014	-0.523798
4	7	-6.282315	-1.026936	-0.350488
5	7	-3.896692	1.034202	0.165762
6	7	-3.825553	-1.162601	-0.252973
7	6	-6.706062	2.570125	-0.327067
8	1	-7.795437	2.556673	-0.319272
9	1	-6.355383	3.197608	-1.150534
10	6	-7.045985	0.125232	-0.189712
11	6	-6.953128	-2.299737	-0.555983
12	1	-7.979590	-2.181673	-0.210222
13	1	-6.961015	-2.578176	-1.617948
14	6	-4.909884	0.826525	-0.864139
15	1	-4.597988	1.314941	-1.795282
16	6	-5.000705	-0.725029	-0.968274
17	1	-4.978425	-1.100944	-1.998564
18	6	-3.256660	2.330049	0.346705
19	1	-2.839921	2.697387	-0.599695
20	1	-2.451544	2.226519	1.073112
21	6	-3.225487	-0.139422	0.445168
22	6	-3.475756	-2.550616	-0.028616
23	1	-3.520406	-3.098462	-0.973228
24	1	-2.457107	-2.574993	0.356107
25	1	-4.138795	-3.029814	0.698961
26	1	-3.975723	3.057652	0.724541
27	1	-6.354535	2.989717	0.620917
28	1	-6.472548	-3.094240	0.016817
29	8	-0.001514	-0.382985	2.887280
30	1	0.769142	-0.318940	2.311888
31	1	-0.758727	-0.469419	2.276033
32	8	2.256259	-0.195352	1.201569
33	8	8.214482	0.254272	0.129054

```
34          7                      3.678878    1.028282   -0.159463
35          7                      4.069275   -1.161159    0.109323
36          7                      6.134167    1.219678   -0.262476
37          7                      6.406580   -0.969946   -0.649494
38          6                      3.136302    2.334357    0.152056
39          1                      2.131570    2.185291    0.546007
40          1                      3.084404    2.939901   -0.756587
41          6                      3.230605   -0.114378    0.474098
42          6                      3.590016   -2.528492    0.212085
43          1                      2.719250   -2.516441    0.867087
44          1                      3.296639   -2.920912   -0.770407
45          6                      4.893334    0.805729   -0.902839
46          1                      4.816027    1.254427   -1.901194
47          6                      5.009236   -0.747619   -0.923353
48          1                      4.733963   -1.196766   -1.885910
49          6                      6.619387    2.586890   -0.334830
50          1                      6.553096    2.977769   -1.358645
51          1                      7.663505    2.575252   -0.023259
52          6                      7.047574    0.172975   -0.212757
53          6                      7.024273   -2.275815   -0.547580
54          1                      6.756495   -2.880869   -1.417767
55          1                      8.103245   -2.126277   -0.528393
56          1                      6.727625   -2.804813    0.364103
57          1                      6.055331    3.240475    0.332502
58          1                      3.732452    2.862553    0.903477
59          1                      4.351194   -3.181051    0.642747
----------------------------------------------------------------
E(RTPSSh) = -1442.54650780 Hartree
Zero-point correction = 0.491094
Thermal correction to Energy = 0.525415
Thermal correction to Enthalpy = 0.526359
Thermal correction to Gibbs Free Energy = 0.417252
Sum of electronic and zero-point Energies = -1442.064492
Sum of electronic and thermal Energies = -1442.030170
Sum of electronic and thermal Enthalpies = -1442.029226
Sum of electronic and thermal Free Energies = -1442.138333
```

References

[1] Y. Lalatonne, C. Paris, J. M. Serfaty, P. Weinmann, M. Lecouvey, L. Motte, *Chem. Comm*., 2008, **22***, 2553–2555.

[2] F. Benyettou, Y. Lalatonne, I. Chebbi, M. Di Benedetto, J. M. Serfaty, M. Lecouvey, L. Motte, *Phys. Chem. Chem. Phys*., 2011, **13***, 10020–10027.

[3] L. Cervera-Gontard, D. Ozkaya, R. Dunin-Borkowski, *Ultramicroscopy*, 2011, **111**, 101–106.

[4] S. Verma, D. Pravarthana, *Langmuir*, 2011, **27**, 13189.

[5] K. M. Park, K. Suh, H. Jung, D. W. Lee, Y. Ahn, J. Kim, K. Baek, K. Kim, *Chem. Commun*., 2009, **1***, 71–73.

[6] F. Geinguenaud, I. Souissi, R. Fagard, L. Motte, Y. Lalatonne, *Nanomed-Nanotechnol.,* 2012**, 8**, 1106–1115.

[7] M. J. Frisch, G. W. Trucks, H. B. Schlegel, G. E. Scuseria, M. A. Robb, J. R. Cheeseman, G. Scalmani, V. Barone, B. Mennucci, G. A. Petersson, H. Nakatsuji, M. Caricato, X. Li, H. P. Hratchian, A. F. Izmaylov, J. Bloino, G. Zheng, Sonnenberg, M. Hada, M. Ehara, K. Toyota, R. Fukuda, J. Hasegawa, M. Ishida, J. L. T. Nakajima, Y. Honda, O. Kitao, H. Nakai, T. Vreven, J. A. Montgomery, Jr., J. E. Peralta, F. Ogliaro, M. Bearpark, J. J. Heyd, E. Brothers, K. N. Kudin, V. N. Staroverov, R. Kobayashi, J. Normand, K. Raghavachari, A. Rendell, J. C. Burant, S. S. Iyengar, J. Tomasi, M. Cossi, N. Rega, N. J. Millam, M. Klene, J. E. Knox, J. B. Cross, V. Bakken, C. Adamo, J. Jaramillo, R. Gomperts, R. E. Stratmann, O. Yazyev, A. J Austin, R. Cammi, C. Pomelli, J. W. Ochterski, R. L. Martin, K. Morokuma, V. G. Zakrzewski, G. A. Voth, P. Salvador, J. J. Dannenberg, S. Dapprich, A. D. Daniels, Ö. Farkas, J. B. Foresman, J. V. Ortiz, J. Cioslowski, D. J. Fox, *Gaussian, Inc.,* Wallingford CT, 2009.

[8] J. M. Tao, J. P. Perdew, *Phys. Rev. Lett*., 2003, **91**, 1–4.

[9] A. Schaefer, C. Huber, R. *J.* Ahlrichs, *Chem. Phys*., 1994, **100**, 5829–5835.

[10] J. F. Stanton, J. Gauss, *Adv. Chem. Phys*., 2003, **125**, 101–146.

[11] A. Montoya, T. N. Truong, A. F. Sarofim, *J. Phys. Chem. A*, 2000, **124**, 6108–6110.